AGU PUBLICATIONS

Geophysical Research Letters

RESEARCH LETTER
10.1002/2016GL068177

Key Points:
- A new mode of internal ocean variability is identified in the Southern Ocean
- It has an important impact on global ocean heat uptake
- It depends on baroclinic instabilities from mesoscale eddies in the Antarctic Circumpolar Current

Supporting Information:
- Movie S2
- Movie S1
- Figure S4
- Figure S3
- Figure S2
- Figure S1
- Movies S1 and S2, and Figures S1–S4 Captions

Correspondence to:
D. Le Bars,
dewi.le.bars@knmi.nl

Citation:
Le Bars, D., J. P. Viebahn, and H. A. Dijkstra (2016), A Southern Ocean mode of multidecadal variability, *Geophys. Res. Lett.*, *43*, 2102–2110, doi:10.1002/2016GL068177.

Received 10 FEB 2016
Accepted 16 FEB 2016
Accepted article online 18 FEB 2016
Published online 7 MAR 2016

A Southern Ocean mode of multidecadal variability

D. Le Bars[1], J. P. Viebahn[1], and H. A. Dijkstra[1]

[1]Institute for Marine and Atmospheric research Utrecht, Department of Physics and Astronomy, Utrecht University, Utrecht, Netherlands

Abstract A 250 year simulation of a strongly eddying global version of the Parallel Ocean Program (POP) model reveals a new mode of intrinsic multidecadal variability, the Southern Ocean Mode (SOM), with a period of 40–50 year. The peak-to-peak difference in the global ocean heat content within a multidecadal cycle is up to 60 ZJ. This change results from surface heat flux variations in the South Atlantic and propagation of temperature anomalies along the Antarctic Circumpolar Current and into the Weddell gyre around 30°E. The temperature anomalies propagate as deep as 5000 m along the isopycnals between 50°S and 30°S and induce multidecadal changes in the Atlantic Meridional Overturning Circulation. A positive feedback loop between the generation of eddies through baroclinic instability and the dynamics of the mean circulation is essential for the existence of the SOM. The dominant physics appears similar to that responsible for variability found in a three-layer quasi-geostrophic eddy-resolving model. This combined with the fact that the SOM is not found in a noneddying version of the same global POP model further suggests that eddy processes are crucial for its existence and/or excitation.

1. Introduction

Over the period 1970–2010, the ocean has absorbed about 93% of the excess heat due to the radiation imbalance at the top of the atmosphere [*Stocker et al.*, 2013]. It is estimated that during this period, the heat content of the upper 700 m ocean has increased by about 170 ZJ and that of the deeper ocean by an additional 80 ZJ. The ocean heat content records, however, show a pronounced multidecadal variability with variations of up to 50 ZJ [*Domingues et al.*, 2008; *Levitus et al.*, 2012; *Balmaseda et al.*, 2013]. There is an ongoing discussion on the magnitude of this observed variability and on the mismatch between climate models and observations [*Gregory et al.*, 2004; *Abraham and Baringer*, 2013; *Cheng and Zhu*, 2014].

The cause of this multidecadal variability is poorly understood although volcanic activity and intrinsic climate variability have been identified as main processes [*Balmaseda et al.*, 2013; *Goddard*, 2014]. The multidecadal variability of the ocean heat content has been held responsible for the relatively low 1998–2010 trend in the global mean surface temperature anomaly, also referred to as the "Global Warming Hiatus" [*Meehl et al.*, 2011, 2013]. While it is clear from observations that multidecadal patterns of sea surface temperature variability exist, e.g., the Atlantic Multidecadal Oscillation [*Schlesinger and Ramankutty*, 1994] and the Pacific Interdecadal Variability [*England et al.*, 2014], the link between these patterns and the global ocean heat content anomalies is far from clear [*Drijfhout et al.*, 2014].

Most studies on climate variability are performed using climate models that do not resolve the internal Rossby deformation radius [*Hallberg*, 2013]. These models generally underestimate multidecadal variations in heat content [*Katsman and Van Oldenborgh*, 2011]. In strongly eddying ocean models that resolve mesoscale features of the ocean circulation, the interaction of baroclinic/barotropic instabilities may lead to intrinsic decadal variability [*Berloff and McWilliams*, 1999; *Berloff et al.*, 2007; *Penduff et al.*, 2011; *Arbic et al.*, 2014; *Sérazin et al.*, 2015]. In particular, using an idealized quasi-geostrophic model, *Hogg and Blundell* [2006] suggest that a positive feedback loop between the generation of eddies though baroclinic instability and the dynamics of the mean circulation leads to multidecadal variability in the Southern Ocean. The presence of eddies in ocean models also provides the "noise" that may excite large-scale instabilities, such as those associated with the thermal Rossby mode [*Frankcombe et al.*, 2010].

Here we analyze results from a 250 years simulation with a strongly eddying state-of-the-art ocean model, forced with seasonal mean atmospheric fields, and report on a new mode of multidecadal variability that we

call the Southern Ocean Mode (SOM). It induces a peak-to-peak variability in global ocean heat content of about 60 ZJ. Eddies are shown to be crucial for the existence/excitation of the SOM and the SOM is indeed absent in a lower resolution (noneddying) version of the same ocean model.

2. Models and Simulations

The global ocean simulations are performed using the Parallel Ocean Program (POP) [*Dukowicz and Smith*, 1994] developed at Los Alamos National Laboratory. The strongly eddying configuration is based on that used by *Maltrud et al.* [2010], with an average 0.1° horizontal resolution and 42 vertical levels. The atmospheric forcing of the model is based on the repeat annual cycle (normal year) Coordinated Ocean Reference Experiment (CORE, see http://www.clivar.org/organization/wgomd/core) forcing data set [*Large and Yeager*, 2004], with 6-hourly forcing averaged to monthly. Wind stress is computed offline using the Hurrell Sea Surface Temperature (SST) climatology [*Hurrell et al.*, 2008] and standard bulk formulae. Evaporation and sensible heat flux were calculated online also using bulk formulae and the model predicted SST. Precipitation was also taken from the CORE forcing data set. Sea ice cover was prescribed based on the −1.8°C isoline of the SST climatology, with both temperature and salinity restored on a timescale of 30 days under diagnosed climatological sea ice.

As initial conditions we used the final state of a 75 years spin-up simulation described in *Maltrud et al.* [2010] using restoring conditions for salinity. The freshwater flux was diagnosed during the last 5 years of this spin-up simulation, and the simulations used here use this diagnosed freshwater flux; no restoring of salinity is used. The model configuration and simulation procedure is discussed in detail in the auxiliary material of *Weijer et al.* [2012]. The simulation analyzed here is the Control Simulation in *Weijer et al.* [2012] which was continued up to model year 325, providing 250 years of data.

The noneddying version of the global POP model has an average 1.0° horizontal resolution and 40 vertical levels and was configured to have a similar Atlantic MOC strength (about 22 sverdrup (10^6 m^3/s) (Sv) at 26°N) as in the strongly eddying version [*Weijer et al.*, 2012; *Toom et al.*, 2014]. The main differences between the high- and low-resolution versions of the model are the type of grids (tripole versus dipole, respectively) and the maximum depth in the model (6000 m versus 5500 m, respectively). In the noneddying version, the Gent and McWilliams scheme [*Gent and McWilliams*, 1990] is used to represent eddy-driven tracer transports. Such a scheme is not needed in the strongly eddying version as these tracer transports are explicitly resolved.

3. The Southern Ocean Mode (SOM)

The strongly eddying POP model displays quite regular multidecadal variability in the global mean temperature (dotted blue curve in Figure 1a), with respect to the mean from years 75 to 325, with a period of 40–50 years. This variability is absent in the low-resolution version of the same model (Figure S1a). Since a bulk formula is used to compute the surface heat fluxes and because there is only seasonal variability in the atmospheric forcing fields, the multidecadal heat flux anomalies are generated by sea surface temperature (SST) anomalies (Figure 1a). A local positive SST anomaly reduces the heat flux toward the ocean, and it appears that this local relation also holds globally in our model simulation. A negative (positive) anomaly in global mean SST leads to an increase (decrease) of the global mean ocean temperature (Figure 1a). To reveal the SOM, it is important to take into account the full depth temperature anomaly because the variability of temperature anomalies in the top 700 m is less regular (dashed red curve in Figure 1a).

When integrated over the full ocean depth, the variability in Ocean Heat Content (OHC) has a peak-to-peak difference of over 60 ZJ (Figure 1b). Time series of OHC variability within the different ocean basins indicate that the largest amplitudes occur in the Southern Ocean (SO) and in the South Atlantic (Figure 1b). However, all basins exhibit regular multidecadal variability in their OHC (Figure 1c). The maximum global OHC variations result from the differently phased contributions of heat storage in different basins with a lag between the OHC in the SO/Indian Ocean and that in the North/South Atlantic. Such phase differences explain why the globally averaged temperature in the top 700 m (Figure 1a) does not exhibit a clear multidecadal variability. While this variability is found in both Northern and Southern Hemispheres with similar amplitudes, both are out of phase (Figure S1b). This is not the case for the fully depth-averaged temperature anomalies because their amplitude is higher in the Southern Hemisphere and the phase shift is only 10 to 15 years (Figure S1c).

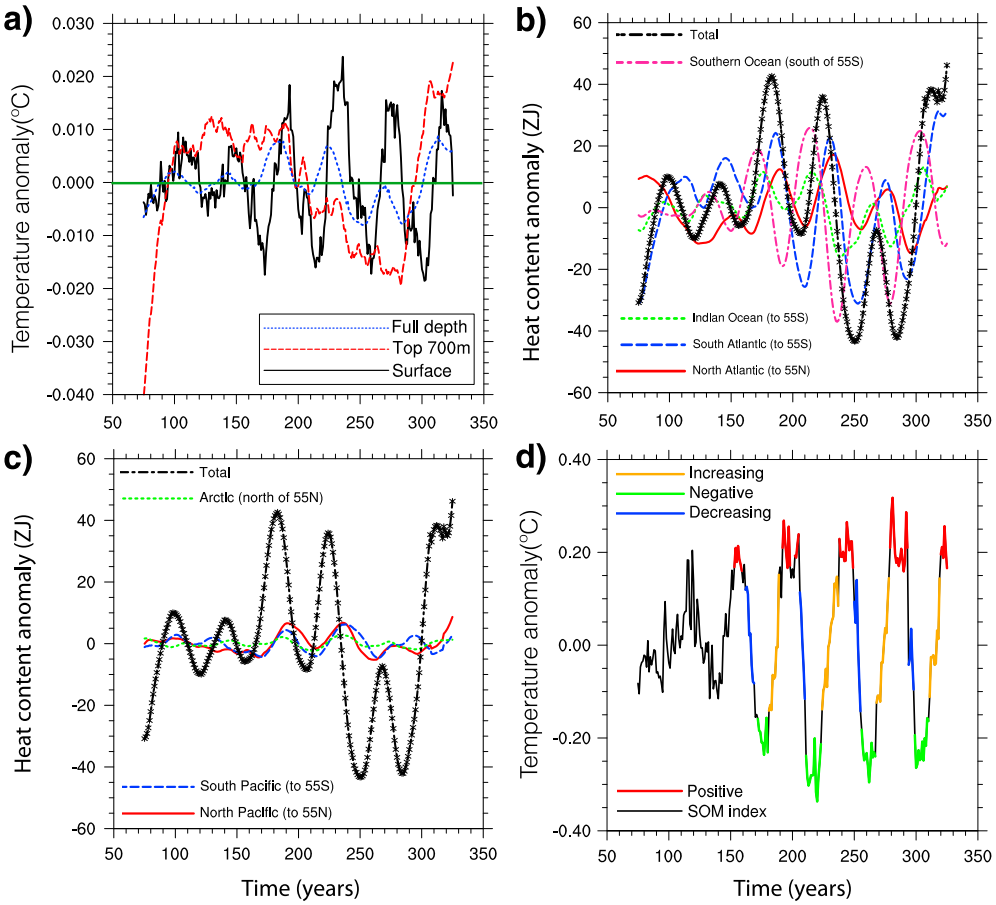

Figure 1. (a) Global mean temperature anomalies (with respect to the 75–325 mean) at the surface (black), top 700 m (red) and over the full depth (blue). (b and c) Full-depth heat content anomalies in different ocean basins. A least square quadratic trend is removed from each time series, and annually averaged data are shown here. (d) Average SST in the area 50°S–35°S, 50°W–0°W (see box in Figure 2a), defined as the Southern Ocean Mode index.

The decadal variability of the sea surface temperature (SST) is particularly strong in the South Atlantic. For this reason, we define a SOM index as the average SST in the area (see box in Figure 2a) between 50°S–35°S and 50°W–0°W (Figure 1d). This region shows variability an order of magnitude bigger than the global mean SST. To describe the SOM, we split the variability into four stages that we will call positive, decreasing, negative, and increasing. The positive phase is composed of the years for which the SOM index is higher than 1 standard deviation, negative is lower than −1 standard deviation, and the decreasing and increasing phases are composed of the intermediate years.

The plots in Figure 2 are composites of all similar SOM phases so they include different decades. We focus here only on the positive and decreasing phases because the anomalies in the negative and increasing phases are similar but with opposite signs. The surface heat flux anomalies associated with the SOM are mainly located in the South Atlantic and in the SO (Figures 2a and 2b). Consistently, the spatial pattern of the temperature anomalies of the SOM is also localized in these basins (Figures 2c and 2d). Here a few decades are enough to store and release massive amounts of heat to a depth of 5000 m (Figures 2e and 2f). Additionally, there are temperature anomalies in the top 1000 m in the whole Atlantic. During a positive SOM phase there is a negative temperature anomaly in the Atlantic sector of the SO between 70°S and 40°S. This pattern is opposite during the negative phase of the mode (Figure S2).

We note that due to the large meanders of the Antarctic Circumpolar Current (ACC) the precise zonal mean pathways of heat transport in the SO depend on the zonal integration paths both in the vertical [*Nurser and Lee*, 2004; *Ferrari and Ferreira*, 2011] and the meridional directions [*Treguier et al.*, 2007; *Viebahn and Eden*, 2012; *Zika et al.*, 2013]. For example, part of the bipolar warming/cooling signal at depth in Figure 2f might be induced

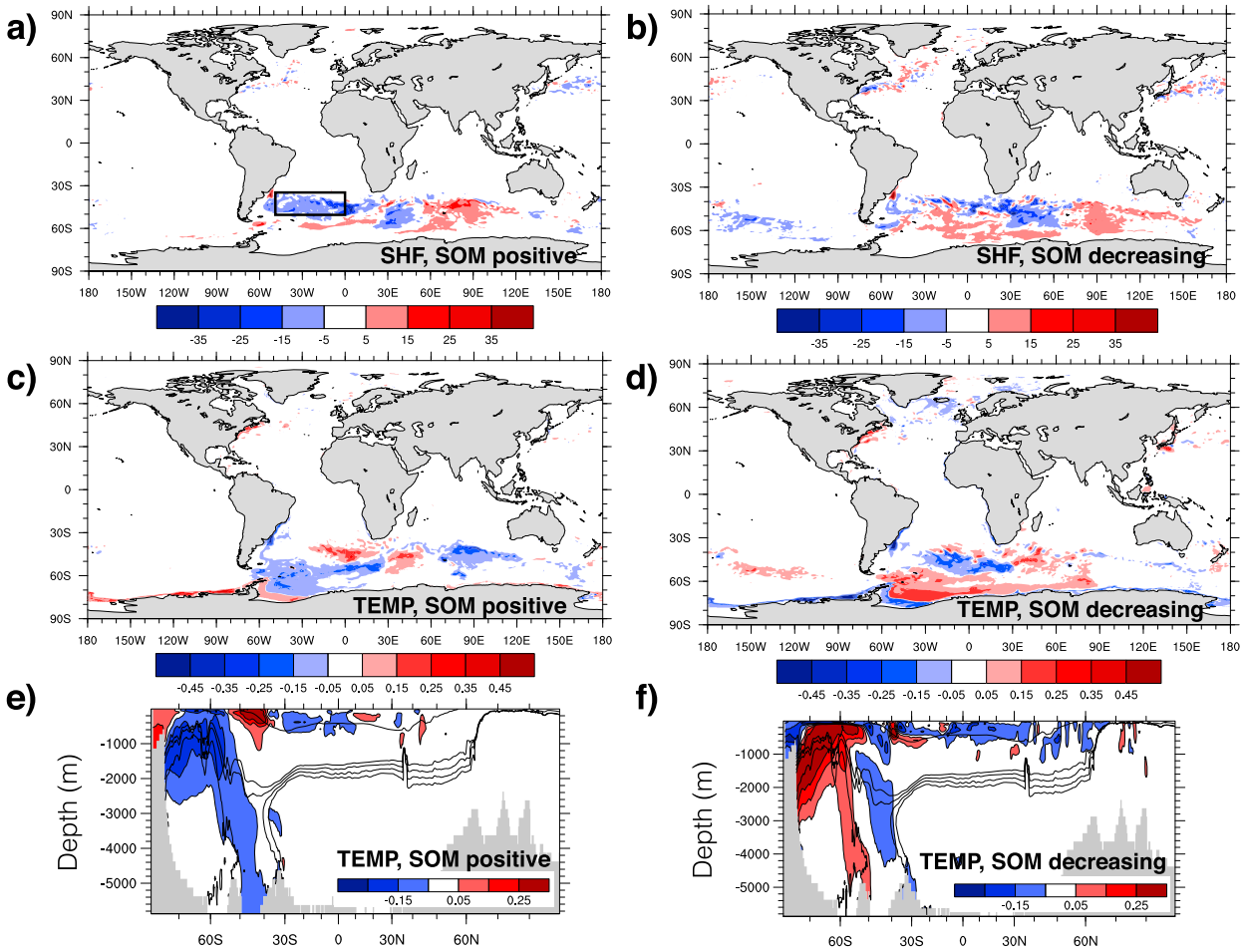

Figure 2. (a and b) Total surface heat flux anomalies, including short wave radiation (units in W/m^2). (c and d) Temperature anomalies (°C), vertically averaged over the full depth. (e and f) Zonally averaged temperature anomalies between 60°W and 0°W, with selected isopycnals in the background. Isopycnals shown have a σ_0 value of 27, 27.82, 27.83, 27.84, and 27.85 kg/m^3. Figures 2a, 2c, and 2e represent the positive phase of the SOM and right ones the decreasing phase. The box in Figure 2a represents the area over which the SST is averaged to compute the SOM index.

by meridional excursions of the ACC instead of actual vertical heat transport. Nevertheless, the presence of large genuine vertical heat transport anomalies below the depth of 700 m is clear from Figure 1a, S1b, and S1c, where temperature anomalies integrated over the full depth have a magnitude similar to those in the top 700 m.

The temperature anomalies of the SOM that occur in the South Atlantic propagate eastward with the ACC (Figure 3a and Movie S1) at a speed of around 0.01 m/s. An advective timescale computed from the transport at Drake Passage (Figure 3c), a depth of 5 km and a width of 20° latitude, has the same order of magnitude. The propagation is smooth in the South Atlantic, but it is interrupted in the south of Africa around 30°E due to the interaction with the Agulhas Current retroflection. In this area, the anomalies split into two parts. The first part continues along the ACC and slowly dissipates and reaches latitudes south of 58° S in the western Indian Ocean. The second part enters the Weddell Gyre (Figure 2b). This might be possible through an increase in cross-stream eddy diffusivity within this area compared to the South Atlantic [*Sallée et al.*, 2008]. Once the anomalies have arrived at the Weddell Gyre (Figure 3b), they propagate westward with a faster speed (0.02 m/s), possibly related to the shallower depth of the anomalies (Figures 2e and 2f). Associated with these anomalies there is also an important variation of the volume transport at Drake Passage, which shows a peak-to-peak difference of up to 18 Sv (Figure 3c).

Once the temperature anomalies have affected the Drake Passage transport via the Weddell gyre, they reenter the South Atlantic. The anomalies then propagate as deep as 5000 m almost adiabatically (Figures 2e and 2f and Movie S2) due to the strong sloping of the isopycnals in the ACC. Note that this downward propagation

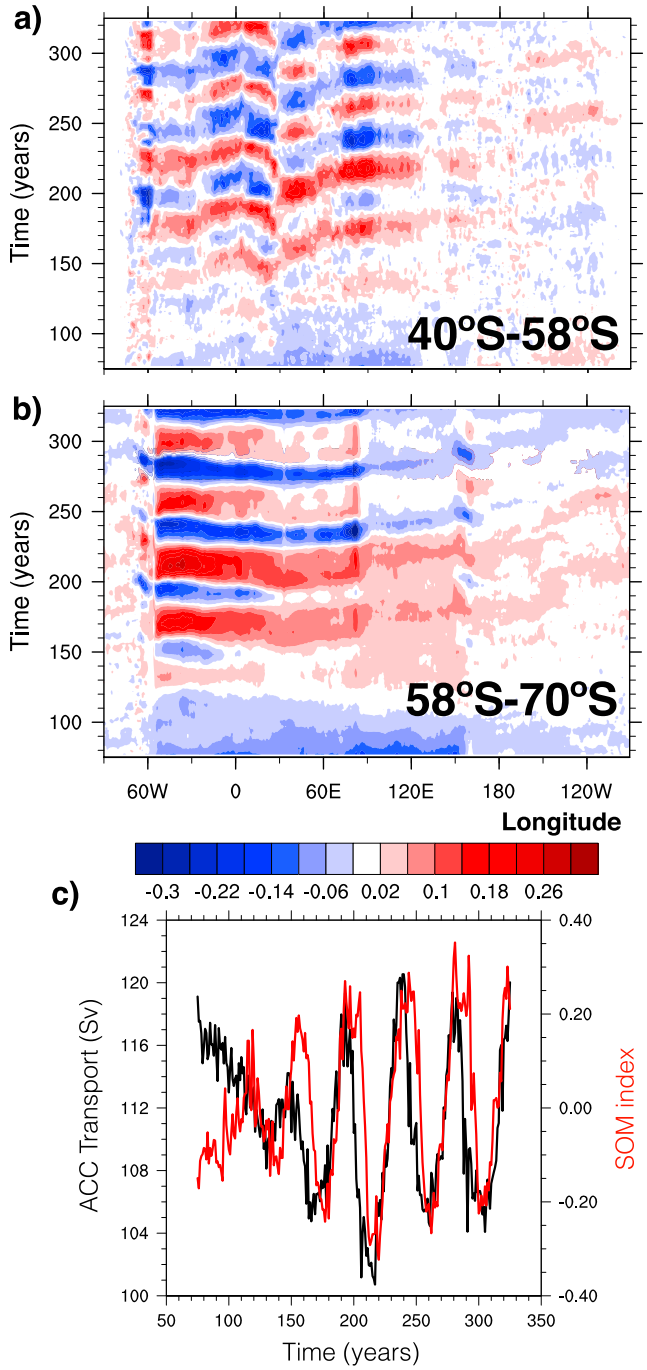

Figure 3. Time/longitude propagation of temperature anomalies (meridionally averaged over the full ocean depth) between (a) 40°S–58°S and (b) 58°S–70°S. The fields are filtered in time with a 5 year running average. (c) Time series of annual mean values of the Antarctic Circumpolar Current (ACC) transport at Drake Passage compared with the SOM index.

is against the temporal mean upwelling in this region forced by the Ekman divergence. This is because heat flux is mostly diffusive in this region [*Gregory*, 2000]. The mechanism of this propagation is a result of the competition between weak upwelling in the temporal mean field and a strong along-isopycnal eddy diffusion *Abernathey et al.* [2013]. In this region of temporal mean upward heat fluxes, an anomalous downward heat flux is the result of weaker upward heat flux. Note that this downward propagation of the heat anomalies is an important component of the peak-to-peak global OHC changes (Figures 1a, S1b, and S1c).

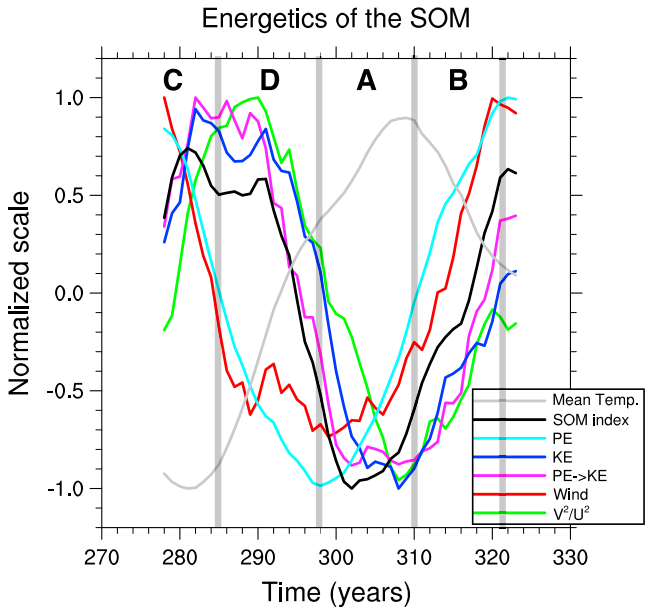

Figure 4. Time series of vertically and horizontally integrated (from 90°S to 30°S) available potential energy (PE), kinetic energy (KE), energy transfer from PE to KE (PE→KE), energy input by the wind, a measure of nonzonality of the flow field (V^2/U^2) where U and V are zonal and meridional velocities, integrated from 90°S to 45°S, from 0°E to 40°E, and between 318 m depth and the surface. All time series represent 5 year running averages. For comparison the SOM index and the spatially mean temperature in the same area are also added to the figure.

Even though the SOM is essentially localized in the Southern Hemisphere, this mode of variability has a major influence on the North Atlantic (Figure 1c) as well. Temperature anomalies propagate northward in the Atlantic basin (Figure S3a) within the upper 1000 m. Multidecadal variations in the maximum of the AMOC stream function are also found (Figure S3b). The anomaly is up to 3 Sv at 30°S and propagates northward while its magnitude decreases.

4. Energetics of the SOM

To identify the physical mechanisms at the origin of the SOM, we diagnose important terms of the mechanical energy budget in a similar way as *Hogg and Blundell* [2006] did for a quasi-geostrophic model. Our formulation of the mechanical energy budget for primitive equations follows *Storch et al.* [2012]. We present the results for one cycle of the SOM in the region south of 30°S. In Figure 4, it is shown that the maxima (minima) in available potential energy (PE) lead maxima (minima) in kinetic energy (KE) such that the two fields are 90° (rather than 180°) out of phase. The energy input by the wind stress forcing is essentially in phase with the PE whereas the energy transfer from PE to KE is approximately in phase with the KE. This behavior of the energetics of the SOM is in complete accordance with the results in *Hogg and Blundell* [2006] (cf. their Figure 12), who found a mode of multidecadal variability in an eddy-resolving three-layer quasi-geostrophic model of a zonal channel flow.

Following *Hogg and Blundell* [2006], the energetics of a SOM cycle is divided into the following four regimes: Regime A represents a state of low total energy starting at the minimum in PE and ending at the minimum in KE. The storage of PE is small in this regime so the production of baroclinic eddies is weak. In regime B, PE builds up until the maximum in PE is reached. This is because the flow is accelerated zonally by the wind stress. Regime C represents a state of high total energy starting at the maximum in PE and ending at the maximum in KE. The flow exceeds a critical threshold for enhanced baroclinic instability which induces an increased generation of eddies by the mean flow. The PE that was stored during regimes A and B is transferred to KE. The enhanced turbulence rearranges the flow field such that there is a loss of correlation between surface ocean velocity and wind stress. Therefore, energy input by the wind stress quickly decreases in regime C. Finally, regime D is defined by decreasing PE and KE. The storage of PE is exhausted so that the conversion of PE to KE begins to abate as well. This is combined with the reduction in energy input by the wind stress forcing, and the system returns to its low-energy state (regime A). It is interesting that the mean temperature in the area

is nearly 180° and 90° out of phase with respect to KE and PE (Figure 4) which indicates a very regular nature of the SOM.

Hogg and Blundell [2006] find that strong eddy activity drives a deep reaching large-scale gyre which produces greater nonzonal flow in all vertical layers, enhancing baroclinic instability. This feature is also found for the SOM (green curve, Figure 4). The spatial pattern of KE anomalies of the SOM (Figure S4) is also comparable to the one found by *Hogg and Blundell* [2006] (cf. their Figure 13). The most dominant dynamic feature is a deep-reaching standing gyre which in our simulation is located in the Weddel gyre region. The gyre is strongest during regime C (presumably driven by eddies), especially in the lower-layer as eddies tend to be more barotropic than the mean flow.

5. Summary and Discussion

We have presented a new mode of intrinsic multidecadal variability, the Southern Ocean Mode (SOM), in a strongly eddying global ocean model. This mode is located in the Southern Ocean, between the South Atlantic and the Weddell Gyre, and has a period of 40–50 years. Anomalies in surface heat flux in the South Atlantic lead to anomalous temperatures that propagate eastward with the ACC and enter the Weddell gyre around 30°E. These anomalies fill up the Weddell gyre and lead to significant changes in ACC transport. They also propagate as deep as 5000 m along the isopycnals between 60°S and 30°S, leading to substantial variability (60 ZJ) in the global OHC.

The mechanism of the SOM is very similar to that of a mode that was found in a three-layer quasi-geostrophic model [*Hogg and Blundell*, 2006], which shows the importance of studies with conceptual models of the Southern Ocean. The generation of mesoscale eddies by baroclinic instability and its impact on the mean flow were shown to be crucial in driving the low-frequency variability. Furthermore, as the SOM is completely absent in the low-resolution (noneddying) version of the same ocean model, the role of eddies and possibly of small-scale flow-topography interactions are thought to be crucial in this intrinsic variability. The pattern of the SOM is localized in the Southern Ocean and is very different from other intrinsic modes of variability which have been found in a noneddying global ocean models, such as the South Pacific Intrinsic Mode *O'Kane et al.* [2013]. The associated variability in the North Atlantic (in particular in the AMOC) seems to be directly caused by the SOM.

An important conclusion of our study is that typical climate models that do not solve the mesoscale eddies in the ocean cannot simulate low-frequency variability such as the SOM. This could have major importance to assess the multidecadal variations of ocean heat content and sea level and their attribution to global warming. One would expect that in a coupled model, the atmospheric damping of SST anomalies would be reduced, giving more freedom to the ocean to evolve freely and possibly strengthening the multidecadal variability. However, one major assumption in ocean-only models forced by atmospheric temperature and bulk formula, is that the atmosphere has an infinite heat capacity. This is of course not realistic given the small heat capacity of the atmosphere compared to the ocean. The capacity of the ocean to absorb and release heat at multidecadal time scales would then reduce in a coupled model, except if it is able to affect the radiative balance at the top of the atmosphere. On the other hand, given the big difference of heat capacity between the ocean and the atmosphere, small variations in OHC can lead to big variations in surface atmospheric temperature. In fact, this might become a dominant effect controlling the multidecadal variability of global mean surface temperature in earth system models when they start to resolve ocean eddies.

The inclusion of a sea ice model would also influence the SOM because important anomalies occur in the Weddell gyre that is mostly covered with ice in the Southern Hemisphere winter months. Sea ice would probably not influence the propagation of temperature anomalies because they are rather deep. One way in which it could have a significant impact would be in changing the amount of solar radiation received by the ocean at its surface. In this case it would probably act as an amplification of temperature anomalies through a positive feedback where warmer water causes less ice and therefore receives more heat.

The question whether the SOM is relevant for the real ocean cannot be answered at the moment due to a lack of observations. Data of the multidecadal variability of deep and bottom water temperatures are not available for the SO. On the other hand, the short data sets available and models using data assimilation techniques both show that the SO is an important region for the global OHC variations [*Purkey and Johnson*, 2010; *Drijfhout et al.*, 2014]. The results here therefore strongly motivate to carry out better and long-term observations of ocean temperatures in the SO.

Acknowledgments
The authors would like to acknowledge two anonymous reviewers for improving the quality of the manuscript. D. Le Bars was funded by the Netherlands eScience Center through the grant 027.012.901 and by the Utrecht University through its strategic theme Sustainability, sub-theme Water, Climate and Ecosystems. The simulations have been performed on the Cartesius supercomputer at SURFsara (https://www.surfsara.nl) through the project SH-284-15. Michael Kliphuis (IMAU-UU) is thanked for his assistance in carrying out the numerical computations with the POP model. The data from the ocean models used in this work are available upon request to the authors.

References

Abernathey, R., D. Ferreira, and A. Klocker (2013), Diagnostics of isopycnal mixing in a circumpolar channel, *Ocean Modell.*, *72*, 1–16, doi:10.1016/j.ocemod.2013.07.004.

Abraham, J., and M. Baringer (2013), A review of global ocean temperature observations: Implications for ocean heat content estimates and climate change, *Rev. Geophys.*, *51*, 450–483, doi:10.1002/rog.20022.

Arbic, B. K., M. Müller, J. G. Richman, J. F. Shriver, A. J. Morten, R. B. Scott, G. Sérazin, and T. Penduff (2014), Geostrophic turbulence in the frequency-wavenumber domain: Eddy-driven low-frequency variability*, *J. Phys. Oceanogr.*, *44*(8), 2050–2069, doi:10.1175/JPO-D-13-054.1.

Balmaseda, M. A., K. E. Trenberth, and E. Källén (2013), Distinctive climate signals in reanalysis of global ocean heat content, *Geophys. Res. Lett.*, *40*, 1754–1759, doi:10.1002/grl.50382.

Berloff, P., A. M. C. Hogg, and W. Dewar (2007), The turbulent oscillator: A mechanism of low-frequency variability of the wind-driven ocean gyres, *J. Phys. Oceanogr.*, *37*(9), 2363–2386, doi:10.1175/JPO3118.1.

Berloff, P. S., and J. C. McWilliams (1999), Large-scale, low-frequency variability in wind-driven ocean gyres, *J. Phys. Oceanogr.*, *29*(8), 1925–1949, doi:10.1175/1520-0485(1999)029<1925:LSLFVI>2.0.CO;2.

Cheng, L., and J. Zhu (2014), Artifacts in variations of ocean heat content induced by the observation system changes, *Geophys. Res. Lett.*, *41*, 7276–7283, doi:10.1002/2014GL061881.

Domingues, C. M., J. A. Church, N. J. White, P. J. Gleckler, S. E. Wijffels, P. M. Barker, and J. R. Dunn (2008), Improved estimates of upper-ocean warming and multi-decadal sea-level rise, *Nature*, *453*(7198), 1090–1093, doi:10.1038/nature07080.

Drijfhout, S. S., A. T. Blaker, S. A. Josey, A. J. G. Nurser, B. Sinha, and M. A. Balmaseda (2014), Surface warming hiatus caused by increased heat uptake across multiple ocean basins, *Geophys. Res. Lett*, *41*, 7868–7874, doi:10.1002/2014GL061456.1.

Dukowicz, J. K., and R. D. Smith (1994), Implicit free-surface method for the Bryan-Cox-Semtner ocean model, *J. Geophys. Res.*, *99*(C4), 7991–8014, doi:10.1029/93JC03455.

England, M. H., S. McGregor, P. Spence, G. A. Meehl, A. Timmermann, W. Cai, A. S. Gupta, M. J. McPhaden, A. Purich, and A. Santoso (2014), Recent intensification of wind-driven circulation in the Pacific and the ongoing warming hiatus, *Nat. Clim. Change*, *4*(3), 222–227, doi:10.1038/nclimate2106.

Ferrari, R., and D. Ferreira (2011), What processes drive the ocean heat transport?, *Ocean Modell.*, *38*(3–4), 171–186, doi:10.1016/j.ocemod.2011.02.013.

Frankcombe, L. M., A. von der Heydt, and H. A. Dijkstra (2010), North Atlantic multidecadal climate variability: An investigation of dominant time scales and processes, *J. Clim.*, *23*(13), 3626–3638, doi:10.1175/2010JCLI3471.1.

Gent, P. R., and J. C. McWilliams (1990), Isopycnal mixing in ocean circulation models, *J. Phys. Oceanogr.*, *20*(1), 150–155, doi:10.1175/1520-0485.

Goddard, L. (2014), Heat hide and seek, *Nat. Clim. Change*, *4*(3), 158–161, doi:10.1038/nclimate2155.

Gregory, J. M. (2000), Vertical heat transports in the ocean and their effect on time-dependent climate change, *Clim. Dyn.*, *16*, 501–515, doi:10.1007/s003820000059.

Gregory, J. M., H. T. Banks, P. A. Stott, J. A. Lowe, and M. D. Palmer (2004), Simulated and observed decadal variability in ocean heat content, *Geophys. Res. Lett.*, *31*, L15312, doi:10.1029/2004GL020258.

Hallberg, R. (2013), Using a resolution function to regulate parameterizations of oceanic mesoscale eddy effects, *Ocean Modell.*, *72*, 92–103, doi:10.1016/j.ocemod.2013.08.007.

Hogg, A. M., and J. Blundell (2006), Interdecadal variability of the Southern Ocean, *J. Phys. Oceanogr.*, *36*, 1626–1645, doi:10.1175/JPO2934.1.

Hurrell, J. W., J. J. Hack, D. Shea, J. M. Caron, and J. Rosinski (2008), A new sea surface temperature and sea ice boundary dataset for the Community Atmosphere Model, *J. Clim.*, *21*(19), 5145–5153, doi:10.1175/2008JCLI2292.1.

Katsman, C. A., and G. J. Van Oldenborgh (2011), Tracing the upper ocean's missing heat, *Geophys. Res. Lett.*, *38*, L14610, doi:10.1029/2011GL048417.

Large, W. G., and S. G. Yeager (2004), Diurnal to decadal global forcing for ocean and sea-ice models: The data sets and flux climatologies, *Tech. Rep.*, NCAR, Boulder, Colo.

Levitus, S., et al. (2012), World ocean heat content and thermosteric sea level change (0–2000 m), 1955–2010, *Geophys. Res. Lett.*, *39*, L10603, doi:10.1029/2012GL051106.

Maltrud, M., F. Bryan, and S. Peacock (2010), Boundary impulse response functions in a century-long eddying global ocean simulation, *Environ. Fluid Mech.*, *10*(1), 275–295.

Meehl, G. A., J. M. Arblaster, J. T. Fasullo, A. Hu, and K. E. Trenberth (2011), Model-based evidence of deep-ocean heat uptake during surface-temperature hiatus periods, *Nat. Clim. Change*, *1*(7), 360–364, doi:10.1038/nclimate1229.

Meehl, G. A., A. Hu, J. M. Arblaster, J. Fasullo, and K. E. Trenberth (2013), Externally forced and internally generated decadal climate variability associated with the interdecadal Pacific oscillation, *J. Clim.*, *26*(18), 7298–7310, doi:10.1175/JCLI-D-12-00548.1.

Nurser, A. J. G., and M.-M. Lee (2004), Isopycnal averaging at constant height. Part I: The formulation and a case study, *J. Phys. Oceanogr.*, *34*, 2721–2739.

O'Kane, T. J., R. J. Matear, M. A. Chamberlain, J. S. Risbey, B. M. Sloyan, and I. Horenko (2013), Decadal variability in an OGCM Southern Ocean: Intrinsic modes, forced modes and metastable states, *Ocean Modell.*, *69*, 1–21, doi:10.1016/j.ocemod.2013.04.009.

Penduff, T., M. Juza, B. Barnier, J. Zika, W. K. Dewar, A.-M. Treguier, J.-M. Molines, and N. Audiffren (2011), Sea level expression of intrinsic and forced ocean variabilities at interannual time scales, *J. Clim.*, *24*(21), 5652–5670, doi:10.1175/JCLI-D-11-00077.1.

Purkey, S. G., and G. C. Johnson (2010), Warming of global abyssal and deep Southern Ocean waters between the 1990s and 2000s: Contributions to global heat and sea level rise budgets*, *J. Clim.*, *23*(23), 6336–6351, doi:10.1175/2010JCLI3682.1.

Sallée, J. B., K. Speer, R. Morrow, and R. Lumpkin (2008), An estimate of Lagrangian eddy statistics and diffusion in the mixed layer of the Southern Ocean, *J. Mar. Res.*, *66*(4), 441–463, doi:10.1357/002224008787157458.

Schlesinger, M. E., and N. Ramankutty (1994), An oscillation in the global climate system of period 65–70 years, *Nature*, *367*(6465), 723–726.

Sérazin, G., T. Penduff, S. Grégorio, B. Barnier, J.-M. Molines, and L. Terray (2015), Intrinsic variability of sea level from Global Ocean simulations: Spatiotemporal scales, *J. Clim.*, *28*(10), 4279–4292, doi:10.1175/JCLI-D-14-00554.1.

Stocker, T., D. Qin, G.-K. Plattner, M. Tignor, S. Allen, J. Boschung, A. Nauels, Y. Xia, V. B. And, and P. M. Midgley (Eds.) (2013), *IPCC, 2013: Climate Change 2013: The Physical Science Basis. Contribution of Working Group I to the Fifth Assessment Report of the Intergovernmental Panel on Climate Change*,1535 pp., Cambridge Univ. Press, Cambridge, U. K., and New York, doi:10.1017/CBO9781107415324.

Storch, J.-S. V., C. Eden, I. Fast, H. Haak, D. Hernández-Deckers, E. Maier-Reimer, J. Marotzke, and D. Stammer (2012), An estimate of the Lorenz energy cycle for the world ocean based on the STORM/NCEP simulation, *J. Phys. Oceanogr.*, *42*(12), 2185–2205, doi:10.1175/JPO-D-12-079.1.

Toom, M. D., H. A. Dijkstra, W. Weijer, M. W. Hecht, M. E. Maltrud, and E. van Sebille (2014), Response of a strongly eddying global ocean to North Atlantic freshwater perturbations, *J. Phys. Oceanogr.*, *44*(2), 464–481, doi:10.1175/JPO-D-12-0155.1.

Treguier, A., M. England, S. Rintoul, G. Madec, J. Le Sommer, and J.-M. Molines (2007), Southern Ocean overturning across streamlines in an eddying simulation of the Antarctic Circumpolar Current, *Ocean Sci.*, *3*(1994), 491–507, doi:10.5194/osd-4-653-2007.

Viebahn, J., and C. Eden (2012), Standing eddies in the Meridional overturning circulation, *J. Phys. Oceanogr.*, *42*(9), 1486–1508, doi:10.1175/JPO-D-11-087.1.

Weijer, W., M. E. Maltrud, M. W. Hecht, H. A. Dijkstra, and M. A. Kliphuis (2012), Response of the Atlantic Ocean circulation to Greenland Ice Sheet melting in a strongly-eddying ocean model, *Geophys. Res. Lett.*, *39*, L09606, doi:10.1029/2012GL051611.

Zika, J. D., et al. (2013), Vertical eddy fluxes in the Southern Ocean, *J. Phys. Oceanogr.*, *43*(5), 941–955, doi:10.1175/JPO-D-12-0178.1.